AD

TECHNICAL REPORT ARCCB-TR-99017

ANALYSIS OF MOLTEN SALT AND SPUTTER-DEPOSITED COATINGS ON STEEL CYLINDERS

S. L. LEE
M. CIPOLLO
D. WINDOVER
C. RICKARD

OCTOBER 1999

US ARMY ARMAMENT RESEARCH,
DEVELOPMENT AND ENGINEERING CENTER
CLOSE COMBAT ARMAMENTS CENTER
BENÉT LABORATORIES
WATERVLIET, N.Y. 12189-4050

REPORT DOCUMENTATION PAGE

Form Approved
OMB No. 0704-0188

1. AGENCY USE ONLY *(Leave blank)*	2. REPORT DATE	3. REPORT TYPE AND DATES COVERED
	October 1999	Final

4. TITLE AND SUBTITLE

ANALYSIS OF MOLTEN SALT AND SPUTTER-DEPOSITED COATINGS ON STEEL CYLINDERS

5. FUNDING NUMBERS

AMCMS No. 6111.01.91A1.1

6. AUTHOR(S)

S.L. Lee, M. Cipollo, D. Windover, and C. Rickard

7. PERFORMING ORGANIZATION NAME(S) AND ADDRESS(ES)

U.S. Army ARDEC
Benet Laboratories, AMSTA-AR-CCB-O
Watervliet, NY 12189-4050

8. PERFORMING ORGANIZATION REPORT NUMBER

ARCCB-TR-99017

9. SPONSORING/MONITORING AGENCY NAME(S) AND ADDRESS(ES)

U.S. Army ARDEC
Close Combat Armaments Center
Picatinny Arsenal, NJ 07806-5000

10. SPONSORING/MONITORING AGENCY REPORT NUMBER

11. SUPPLEMENTARY NOTES

Presented at the 26th International Conference on Metallurgical Coatings and Thin Films, San Diego, CA, 12-16 April 1999.
Published in *Surface Coatings and Technology.*

12a. DISTRIBUTION/AVAILABILITY STATEMENT

Approved for public release; distribution unlimited.

12b. DISTRIBUTION CODE

13. ABSTRACT *(Maximum 200 words)*

Prototype tantalum coatings, electrochemically deposited from a molten salt onto 20-mm interior bore steel liners, exhibited superior wear and erosion behavior compared to chromium coatings. The liners were subjected to cyclic exposures of high temperature, pressure, and an aggressive chemical environment. X-ray analysis of the coatings revealed a low-hardness, randomly-oriented, body-centered-cubic, α-phase tantalum. Formation of tantalum oxides (predominantly Ta_2O_5), swaging due to the low-hardness of the coatings, a 2-μm layer consisting of tantalum and carbon at the tantalum/steel interface, and surface compressive residual stresses were observed. Cylindrical magnetron sputtering systems were constructed to coat 45-mm interior bore steel cylinders to protect them from wear and erosion. X-ray diffraction, scanning electron microscopy, photomicrography, and hardness analysis of several sputter-deposited tantalum specimens revealed coatings consisting of soft body-centered-cubic α-phase and hard tetragonal β-phase tantalum.

14. SUBJECT TERMS

Molten Salt Deposition, Cylindrical Magnetron Sputtering Deposition, Tantalum, Thick Refractory Coatings

15. NUMBER OF PAGES

23

16. PRICE CODE

17. SECURITY CLASSIFICATION OF REPORT	18. SECURITY CLASSIFICATION OF THIS PAGE	19. SECURITY CLASSIFICATION OF ABSTRACT	20. LIMITATION OF ABSTRACT
UNCLASSIFIED	UNCLASSIFIED	UNCLASSIFIED	UL

DISCLAIMER

The findings in this report are not to be construed as an official Department of the Army position unless so designated by other authorized documents.

The use of trade name(s) and/or manufacturer(s) does not constitute an official endorsement or approval.

DESTRUCTION NOTICE

For classified documents, follow the procedures in DoD 5200.22-M, Industrial Security Manual, Section II-19, or DoD 5200.1-R, Information Security Program Regulation, Chapter IX.

For unclassified, limited documents, destroy by any method that will prevent disclosure of contents or reconstruction of the document.

For unclassified, unlimited documents, destroy when the report is no longer needed. Do not return it to the originator.

TABLE OF CONTENTS

TABLES

LIST OF ILLUSTRATIONS

ACKNOWLEDGEMENTS

The authors wish to thank G. D'Andrea, J. Vasilakis, and P. Cote for their interest and support.

INTRODUCTION

Tantalum is deposited in two phases: a body-centered-cubic α-phase (Im3m space group), and a metastable tetragonal β-phase (P42/mnm space group). Bulk tantalum, predominately α-phase, possesses good chemical, thermal, and mechanical properties, including a high melting temperature of 2996°C, elastic modulus similar to that of substrate steel, good ductility and formability, and resistance to aggressive hot propellant gases. The physical properties of β-phase tantalum are not well known, except that it is hard, brittle, thermally unstable, and transforms into α-phase tantalum at 750° to 1000°C.

Mellors and Senderoff (refs 1-3) have described a molten salt process for depositing dense, high purity, refractory metals including tantalum. Then Cullinan *et al.* (ref 4), Ahmad *et al.* (ref 5), and Aalto *et al.* (ref 6) applied the technique to study wear and erosion in 20-mm and 105-mm interior bore liners. Figure 1 shows the results after liners were subjected to cyclic exposure of high-pressure, hot propellant gases during firing tests. The wear remained low in tantalum-coated liners, but increased greatly with rounds fired in chromium-coated liners. Ahmad *et al.* (ref 7) further reported that tantalum-chromium alloys deposited from molten salt resulted in increased microhardness compared to the pure tantalum metal. However, only limited photomicrography and hardness data were available from these studies. Thompson and Pan (ref 8) electroplated tantalum specimens from molten salt on copper plates and observed both α- and β- phases. Holloway and Fryer (ref 9) and Catania *et al.* (ref 10) studied the potential application of tantalum thin films as a diffusion barrier against copper diffusion in semiconductors. Clevenger *et al.* (refs 11,12) studied the β- to α- phase transformation and stress relaxation in sputtered tantalum thin films. Cabral *et al.* (ref 13) reported that during thermal cycling, β-phase tantalum thin films exhibited highly compressive stress and became extremely brittle.

Cylindrical magnetron sputtering systems were constructed to perform high rate sputtering of refractory coatings onto cylinders with large length-to-diameter ratios. Cox and McClanahan (ref 14) studied high-rate sputtering of tantalum at temperatures under 500°C and concluded that the process can produce adherent defect-free uniform coatings on 120-mm steel cylinders. Matson *et al.* (ref 15) reported that triode-sputtered tantalum on a 120-mm steel cylinder with a niobium interface layer produced all α-phase tantalum coatings. Lee and Windover (ref 16) characterized the triode-sputtered coatings and found surface and interstitial oxygen, α-phase tantalum, tensile surface stresses, and preferred [110] orientation with in-plane anisotropy.

High temperature molten salt deposition is an established plating process. However, its application to high temperature wear and erosion of cylindrical structures has not been fully explored. This study demonstrates that such coatings are low-hardness, ductile, randomly-oriented, cubic α-phase tantalum. Formation of tantalum oxides, surface compressive residual stresses, a layer of hard tantalum carbide of 2-μm thickness at the tantalum/steel interface, swaging of the coatings, and fatigue cracks all play roles in wear and erosion of tantalum. Magnetron sputtering deposition of environmental-friendly refractory coatings on the interior bore of cylinders is a new technology currently under development in our laboratory. The analysis of several sputtered tantalum specimens showed mixtures of low-hardness, body-

centered-cubic α- and hard tetragonal β- tantalum phases. The microstructure was *zone 1* and *zone T* in Thornton's structure model (refs 17-19). Our results provide input to the design and development of future refractory coatings for full-length (4.5-m) cylinders.

MOLTEN SALT ELECTROCHEMICAL DEPOSITION PROCESS

Figure 2a displays the electrolyte cell used to plate tantalum on the steel liners, showing the tantalum anode and the cylindrical liner as cathode. Figure 2b shows the liner-cylinder assembly. Figure 2c is a schematic of tube rifling showing the distinction between lands and grooves seen in cross-sectional photomicrographs. The 'liner technology' was developed because the 700° to 850°C molten salt temperature can cause degradation in the mechanical properties of the substrate steel. Several reports have described the engineering of liners, the electrochemical molten salt deposition process, shrink-fit operation, and subsequent firing tests (refs 4-6). The electrolyte used in the deposition was a eutectic mixture of LiF–NaF–KF (FLiNaK), to which 5 to 10% K_2TaF_7 was added. For maximum anode and cathode efficiency, the salts must be free of moisture, oxides, and the other halogens. Senderoff *et al.* (ref 3) suggested that the following intermediate reversible process produced insoluble TaF_2, which interferes with the dendritic growth by providing additional nucleation sites to give dense coatings. The final irreversible process produces tantalum. Table 1 gives the specifications for the two liners in this investigation.

$$(TaF_7)^{-2} + 3e \Leftrightarrow TaF_2 + 5F^-$$
$$TaF_2 + 2e \Rightarrow Ta + 2F^-$$

Table 1. Tantalum Liners Deposited in Molten Salt

	Length (cm)	Inside Diameter (mm)	Ta Thickness (μm)	Rounds Fired
Liner 1	20	20	76	1097
Liner 3	20	20	127	5034

CYLINDRICAL MAGNETRON SPUTTERING DEPOSITION FOR CYLINDERS

Figure 2d is a schematic showing the cylindrical magnetron sputter deposition system. It consists of a water-cooled, current-carrying conductor (CCC), surrounded by a 99.995% pure tantalum target located at the center of a coaxial cylindrical substrate. The target acts as the cathode, and the cylinder acts as the anode and vacuum vessel. The substrate is water-cooled and maintains a constant temperature. A magnetic field, $\boldsymbol{B}$, around the CCC, when combined with the electric field, $\boldsymbol{E}$, in the radial direction causes electron motion in the $\boldsymbol{E} \times \boldsymbol{B}$ direction. This interaction encourages ionization in the small annular gaps. The current system is capable of a predeposition base pressure of 1.3×10^{-5} Pa (1×10^{-7} Torr). The sputtering gas is 99.999% pure argon. Argon pressures of 0.13 to 33 Pa (1 to 250 mTorr) and plasma power of 500 to 3000 watts were used. High deposition rate sputtering, on the order of 25 μm/hr, and coating thicknesses up to 250 μm on 45-mm cylinders were reached. Table 2 lists the cylindrical magnetron sputter-deposited specimens under investigation.

Table 2. Cylindrical Magnetron Sputtered Tantalum Coatings

	Cylinder Inside Diameter (mm)	Argon Gas Pressure (Pa)	Substrate Temperature (°C)	Coating Thickness (μm)
Ta13a	45	12-13	100	15
Ta13b	45	12-13	350	28
Casius	45	33	NA*	125
Tri-Layer	45	20/13/9	NA*	50

*Not Available.

X-RAY AND PHOTOMICROGRAPH CHARACTERIZATION TECHNIQUES

X-ray diffraction analysis was performed using Cu radiation on a Scintag PTS2000 diffractometer. The x-ray scan range was $2\theta = 5°$ to $162°$. X-ray stress analysis was performed using Cr radiation reflecting from the [220] planes of tantalum $2\theta = 157.13°$ on a TEC stress analyzer. For specimens with small radius of curvature, such as the liners with 20-mm inside diameter, diffraction scans were performed in both the longitudinal and hoop directions to avoid specimen geometry related distortions (see Figure 2c). Energy dispersive x-ray fluorescence, photomicrography at magnifications of 50× to 1000×, and scanning electron microscopy up to 50,000× complemented the x-ray diffraction analysis. Photomicrography of cross sections was used to reveal the differences in color and texture brought out by polishing. The harder β-phase tantalum appears lighter, and the softer α-phase tantalum appears darker in the optical photomicrograph. A laser photomicrograph using a confocal microscope was also obtained. Hardness was measured using a diamond indentor on a Leitz microhardness tester and a diamond pyramid on a Leco M400 microhardness tester. High-resolution pole figure analysis for the molten salt specimens was performed, but it is not included in this report.

MOLTEN SALT TANTALUM-COATED STEEL LINERS

Liner 3—20-cm long and 20-mm diameter—was coated with 127 μm of tantalum, and exposed to 5034 cycles consisting of temperatures above 1000°C and pressures above 700 MPa. After firing, it was sectioned axially into eight pieces. Figure 3a compares the x-ray diffraction patterns of two specimens cut 7.5-cm and 10-cm from the breech end of the liner. X-ray data disclosed surface α-phase tantalum, tantalum oxide (predominantly Ta_2O_5), copper debris (which came from the fired projectiles), and weak steel peaks. Figure 3b shows the ratio of x-ray diffraction tantalum oxide intensity-to-tantalum intensity along the axial direction for Liner 3. Diamonds represent the relative intensity of the Ta_2O_5 peak at $2\theta = 28°$ to the tantalum peak at $2\theta = 38°$. Dots give the intensity of the sum of all tantalum oxide peaks relative to the total intensity of the tantalum peaks. The graph shows that oxidization was higher near the breech end, and fell off at approximately 9-cm from the breech, reflecting the variation of operation temperature and pressure along the liner axis.

Liner 1—20-cm long and 20-mm diameter—was coated with 76 μm tantalum, and exposed to 1097 thermal cycles. The x-ray diffraction patterns of Liner 1 were very similar to those of Liner 3. The intensity ratio of the Ta_2O_5 peak in Liner 3-to-Liner 1 was 1.7. This demonstrated that oxidation of tantalum depends on the operation history, and increases with rounds fired.

X-ray stress analysis of Liner 3 after 5034 rounds revealed approximately 280 MPa compressive residual stress toward the breech end and 560 MPa compressive residual stress toward the muzzle end. Figure 3c shows the $\sin^2(\psi)$ curves, which were relatively linear because of the random crystalline orientation in molten salt-deposited tantalum. Stress measurements were performed in the groove area of the liners in the axial direction. Deposition residual stresses in the axial and hoop directions were not expected to vary significantly, but the radius-of-curvature and the liner geometry made it difficult to perform hoop stress determination and thereby verify the data.

Figure 4a shows a photomicrograph of Liner 1 after sectioning, mounting, polishing, and etching. The figure shows a uniform, all α-phase tantalum coating with columnar growth, and surface copper debris. A 'swaging effect' resulting in an enlarged land section and a diminished groove section can also be seen. Note the ductility of tantalum allowed it to flow accordingly. Figure 4b is a photomicrograph of Liner 1, showing that the fatigue cracks are likely to occur near the land-to-groove transition region with very high plastic strain. Figure 4c shows the photomicrograph of Liner 3 giving hardness measurements performed. The average thicknesses of the eight sections in Liner 3 were 112 μm in the land, 90 μm in the groove, and 148 μm in the thickest swaged areas.

Figure 4d is a scanning electron micrograph depicting a piece of tantalum encased in melted copper. A crack initiated at the sharp edges of the casing, propagated toward the interface, and generated a pronounced crack in the steel substrate and a crack along the interface. Figure 4e is scanning electron micrograph depicting a crack that was initiated at the coating surface. The crack propagated through the thickness of the coating and generated a wider crack in the steel and a smaller horizontal crack along the interface. The wider crack width in the steel indicates that steel is much less resistant to high temperature and pressure chemical attack. Energy dispersive x-ray analysis showed copper, tantalum, and steel in the cracks. Fine copper particles were also observed in the horizontal crack along the interface.

Figures 4d and 4e show a 2-μm thick interface layer between tantalum coatings and steel substrate. This interface layer was previously observed in a molten salt coating with a hardness of ~640 $Vickers_{50}$ (~790 KHN_{50}), but was not identified (ref 5). Our energy dispersive x-ray analysis of this layer using a 5 kV electron beam at 30,000× magnification disclosed tantalum and carbon in the layer. Carbon is believed to evolve from the steel substrate surface during tantalum deposition, and its concentration should increase with temperature. Hardness measurements included ~240 $Vickers_{50}$ (~294 KHN_{50}) in molten salt α-phase tantalum, 810 to 1000 $Vickers_{50}$ (1000 to 1220 KHN_{50}) in molten salt β-phase tantalum, and ~390 $Vickers_{50}$ (~480 KHN_{50}) in the steel substrate.

CYLINDRICAL MAGNETRON SPUTTERED TANTALUM COATINGS

Figure 5a reveals the surface x-ray diffraction scans of two specimens cut from the same cylinder deposited at 12 and 13 Pa (90 to 100 mTorr) argon pressure. Ta13a was deposited at ~150°C, and Ta13b at ~400°C substrate temperature. Ta13a, deposited at the lower temperature, showed predominantly β-phase tantalum, characterized by the strong preferred [002] orientation. Ta13b, deposited at the higher temperature, showed predominantly α-phase tantalum, with a small concentration of β-phase tantalum, again characterized by the [002] orientation. Figure 5b reveals the microstructure for Ta13a. The microstructure exhibited coarse and fine growth columns with extensive voids. The topography, seen in Figure 5c, included dome-topped structures with voids. The specimen was a typical *zone 1* porous structure as described by Thornton (refs 17-19). Figure 5d reveals the microstructure of Ta13b. This microstructure showed nucleation in the β-phase, and growth of the fan-shaped α phase. The topography of the polished and etched Ta13b surface, found in Figure 5e, included smooth facets with dimension on the order of 1μm. Hardness measured ~344 $Vickers_{50}$ (~426 KHN_{50}), in Ta13b, using a diamond pyramid on a Leco M400 microhardness tester. This value is close to, but higher than the ~281 $Vickers_{50}$ (~350 KHN_{50}) hardness reported for bulk α-phase tantalum. The higher value was due to the small β-phase component in the Ta13b specimen. Hardness in β-phase, Ta13a was ~820 $Vickers_{50}$ (~1009 KHN_{50}).

Figure 6a presents the x-ray diffraction of two other cylindrical magnetron sputter-deposited specimens. The top pattern is from a 50-μm tri-layer coating, which was sputtered at 20, 13, and 9 Pa (150, 100, and 70 mTorr). The pattern shows surface β-phase tantalum and a doublet peak at $2\theta = 40°$. Nitrogen purging was used at the end of the deposition of the tri-layer coating to prevent oxidation, which may form surface tantalum nitrides. The second pattern is for the Casius coating deposited at 33 Pa (250 mTorr). It shows surface β-phase tantalum with broadened diffraction peaks compared to the tri-layer coating. Microstrain and particle size can introduce diffraction peak broadening. Kinetic processes in sputtering control the physical characteristics of the coatings. Figure 6b demonstrates that coating morphology changed with changing argon pressure in the tri-layer coating: bottom layer at 20 Pa (150 mTorr), middle layer at 13 Pa (100 mTorr), top layer at 9 Pa (70 mTorr). Figure 6c is a laser photomicrograph of the specimen taken at 33 Pa (250 mTorr) showing coating porosity. This coating has a density of 10.5 gm/cm^3 calculated from weight loss of the target. At high argon pressure, porosity is expected due to the atomic shielding effect of the argon atoms.

DISCUSSION

Cullinan *et al.* (ref 4) have demonstrated that molten salt tantalum liners exhibited superior wear and erosion performance compared to chromium-coated liners in firing test results. Their study suggested that tantalum is an excellent choice of material for high temperature wear and erosion. Phase is the most important factor controlling coating performance. The current work revealed successful molten salt-deposited tantalum liners consisting of a soft, randomly oriented body-centered-cubic α-phase tantalum. Ahmad *et al.* (ref 5) reported on α-phase tantalum in as-deposited molten salt tantalum liners, and problems with liners containing β-phase tantalum. However, our sputtered tantalum showed mixtures of α- and β-, or all β- tantalum

phases. Sputtering parameters control the structure and morphology in sputtered coatings. Purity of sputtering gas, substrate nature, substrate temperature, and substrate bias can affect tantalum nucleation and growth.

Westwood and Livermore (ref 20) proposed that the tetragonal β-phase tantalum is an impurity-stabilizing phase that is formed to accommodate impurities in the coatings at levels higher than the solubility limit for the body-cubic-centered α-phase tantalum. Feinstein and Hutteman (ref 21) concluded that the β-phase always resulted on substrates that contain oxygen or have a surface oxide. Substrates that have a high resistance to oxidation always nucleated in the α-phase, and included gold, platinum, rhodium, beryllium, and tungsten (ref 22). Face and Prober (ref 23) described deposition of α-phase tantalum using a niobium interface layer. Matson *et al.*(ref 15) and Lee and Windover (ref 16) reported triode-sputtered tantalum with a niobium interface layer produced all α-phase tantalum coatings on steel cylinders, but adhesion improvement was needed. Current nano-electronics research uses tantalum thin films as a diffusion barrier, where α-phase tantalum is the preferred phase. Colgan and Fryer (ref 24) revealed that an interface layer of Ta(N) promoted the growth of α-phase tantalum thin films. Stavrev *et al.* (ref 25) reported a transition from tetragonal β-phase tantalum to body-centered-cubic Ta(N) with the addition of N_2 to the sputtering gas.

Substrate temperature is extremely important in controlling phase, density, microstructure, stress, and texture in nucleation and growth of coatings. Thornton (refs 17-19) has predicted a porous *zone 1* structure resulting from depositions at high sputtering gas pressure and low temperature. Tantalum has a high melting temperature of 2996°C. In order to avoid degrading substrate steel, a substrate temperature below 500°C should be considered. At this temperature, T/T_m is less than 0.17, allowing only *zone 1* and *zone T* structures. In the transition region, higher substrate temperature promotes growth of the *zone T* structure. Schauer and Roschy (ref 26) reported that high substrate temperature favors growth of α-phase tantalum. In this work, cylindrical magnetron-sputtered Ta13b deposited at a higher temperature showed a preferred α-phase tantalum and improved microstructure compared to Ta13a, which showed porous, all β-phase tantalum.

Residual stresses can cause cracking, buckling, and delamination. Compressive surface residual stresses were observed in the after-fired molten salt tantalum coating surface, however no prefired specimens were available for residual stress measurement comparison. Moderate compressive residual stresses on the coating surface in a tensile loading environment during operation may be more advantageous compared to tensile residual stresses. Thornton *et al.* (refs 27,28) observed very high internal stresses between 2.5 GPa compressive to 2.0 GPa tensile as a function of sputtering gas pressure in sputtered depositions.

As-deposited, chromium coatings are known to suffer from extensive crack networks, which result from high internal stresses during deposition. During operation, the crack network grows due to the high mechanical and thermal stress cycling and the aggressive chemical environment. Hot propellant gases, such as CO, CO_2, H, H_2O, N_2, NO, H_2S, etc., penetrate the cracks and interact with the substrate causing failure in the coatings and substrate. In the molten salt tantalum deposition here, the soft body-centered cubic tantalum flowed and as such,

deposition cracks were rarely observed. However, fatigue stress cracks were generated in the molten salt tantalum during the cyclic high temperature tensile stress loading, which allowed the hot gases to penetrate into the steel substrate.

Oxidation of tantalum was observed in molten salt-deposited tantalum, and in triode-sputtered tantalum in our previous work (ref 16). Tantalum oxidizes to form predominantly Ta_2O_5 at 1400°C. Ta_2O_5 has a melting point temperature of 1872°C, and is moderately passivating. Our current work discovered that oxide formation increases with the number of rounds fired. As shown in Figure 1, the increasing oxides do not cause further degradation of the coatings or the substrate.

CONCLUSIONS

1. The molten salt tantalum-coated steel liners showed low-hardness ~237 $Vickers_{50}$ (~296 KHN_{50}), a body-centered-cubic structure, random crystalline orientation, good ductility, and surface compressive residual stresses.

2. Cylindrical magnetron sputter-deposited tantalum coatings on the interior surfaces of steel cylinders had a mixture of α- and β- phases, or all β-phase. The specimens showed *zone 1* and *zone T* microstructure. Changing sputtering gas pressure significantly affected the coating morphology.

3. Current results demonstrate that elevated substrate temperatures promote the growth of α-phase tantalum with a *zone T* microstructure.

4. Oxidation of tantalum increases with increasing rounds of operation. The percentage of oxidation also depends on the axial location in the liner.

5. Wear and erosion behavior in molten salt tantalum coatings is superior compared to chromium coatings because there are no deposition cracks; soft and ductile tantalum allows material flow with fewer fatigue cracks. Additionally, oxidation of tantalum does not cause further wear and erosion.

REFERENCES

1. Mellors, G.W., and Senderoff, S., Union Carbide, U.S. Patent 3444058, 1969; Canadian Patent 658546, 1964.

2. Senderoff, S., *Metallurgical Reviews*, No. 106, 1966, p. 97.

3. Senderoff, S., Mellors, G.W., and Reinhart, W.J., *Journal of the Electrochemical Society*, Vol. 112, No.8, 1965, p. 840.

4. Cullinan, R.L., D'Andrea, G., Croteau, P., and Arnold, C., U.S. Army Technical Report ARLCB-TR-80027, Benet Laboratories, Watervliet, NY, December 1980; also Cullinan, R.L., D'Andrea, G., and Croteau, P., U.S. Army Technical Report ARLCB-TR-81011, Benet Laboratories, Watervliet, NY, April 1981.

5. Ahmad, I., Barranco, J., Aalto, P., and Cox, J., U.S. Army Technical Report ARLCB-TR-83029, Benet Laboratories, Watervliet, NY, September 1983.

6. Aalto, P.D., O'Hara, G.P., and D'Andrea, G., Benet Internal Technical Report BWL 83-2, Benet Laboratories, Watervliet, NY, June 1983.

7. Ahmad, I., Spiak, W.A., and Janz, G.J., *Journal of Applied Electrochemistry*, Vol. 11, 1981, p. 291.

8. Thompson, J.F., and Pan, S.K., U.S. Army Technical Report ARCCB-TR-90028, Benet Laboratories, Watervliet, NY, October 1990.

9. Holloway, K., and Fryer, P.M., *Applied Physics Letters*, Vol. 57, No. 17, 1990, p. 1736.

10. Catania, P., Doyle, J.P., and Cuomo, J.J., *Journal of Vacuum Science and Technology A*, Vol. 10, No. 5, 1992, p. 3318.

11. Clevenger, L.A., Bojarczuk, N.A., Holloway, K., Harper, J.M.E.,Cabral, C., Jr., Schad, R.G., Cardone, F., and Stolt, L., *Journal of Applied Physics*, Vol. 73, No. 1, 1993, p. 300.

12. Clevenger, L.A., Mutscheller, A., Harper, J.M.E., Cabral, C., Jr., and Barmak, K., *Journal of Applied Physics*, Vol. 72, No. 10, 1992, p. 4918.

13. Cabral, C., Jr., Clevenger, L.A., and Schad, R.G., *Journal of Vacuum Science and Technology B*, Vol. 12, No. 4, 1994, p. 2818.

14. Cox, J.F., and McClanahan, E.D., *Proceedings of the Tri-Service Gun Tube Wear and Erosion Symposium*, 1982, p. 277.

15. Matson, D.W., Merz, M.D., and McClanahan, E.D., *Journal of Vacuum Science and Technology A*, Vol. 10, No. 4, 1992, p. 1791.

16. Lee, S.L., and Windover, D., U.S. Army Technical Report ARCCB-TR-98012, Benet Laboratories, Watervliet, NY, July 1998.

17. Thornton, J.A., *Annual Review of Materials Science*, Vol. 7, 1977, p. 239.

18. Thornton, J.A., and Penfold, A.S., *Thin Film Processes*, (J.L. Vossen and W. Kern, Eds.), Academic Press, 1978, p. 75.

19. Thornton, J.A., *Semiconductor Materials and Process Technology Handbook*, (G.E. McGuire, Ed.), Noyes Publications, 1988, p. 329.

20. Westwood, W.D., and Livermore, F.C., *Thin Solid Films*, Vol. 5, 1970, p. 407.

21. Feinstein, L.G., and Hutteman, R.D., *Thin Solid Films*, Vol. 16, 1973, p. 129.

22. Schwartz, N., and Feit, E.D., *Journal of the Electrochemical Society: Solid State Science and Technology*, Vol.124, No. 1, January 1977, p. 123.

23. Face, D.W., and Prober, D.E., *Journal of Vacuum Science and Technology A*, Vol. 5, No. 6, 1987, p. 3408.

24. Colgan, E.G., and Fryer, P.M., Internal Patent Publication No. WO 92/07968, IBM Corporation, 1992.

25. Stavrev M., Fischer, D., Wenzel, C., Drescher, K., and Mattern, N., *Thin Solid Films*, Vol. 307, 1997, p. 79.

26. Schauer A., and Roschy, M., *Thin Solid Films*, Vol. 12, 1972, p. 313.

27. Thornton, J.A., Tabock, J., and Hoffman, D.W., *Thin Solid Films*, Vol. 67, 1979, p. 111.

28. Thornton, J.A., and Hoffman, D.W., *Thin Solid Films*, Vol. 171, 1989 p. 5.

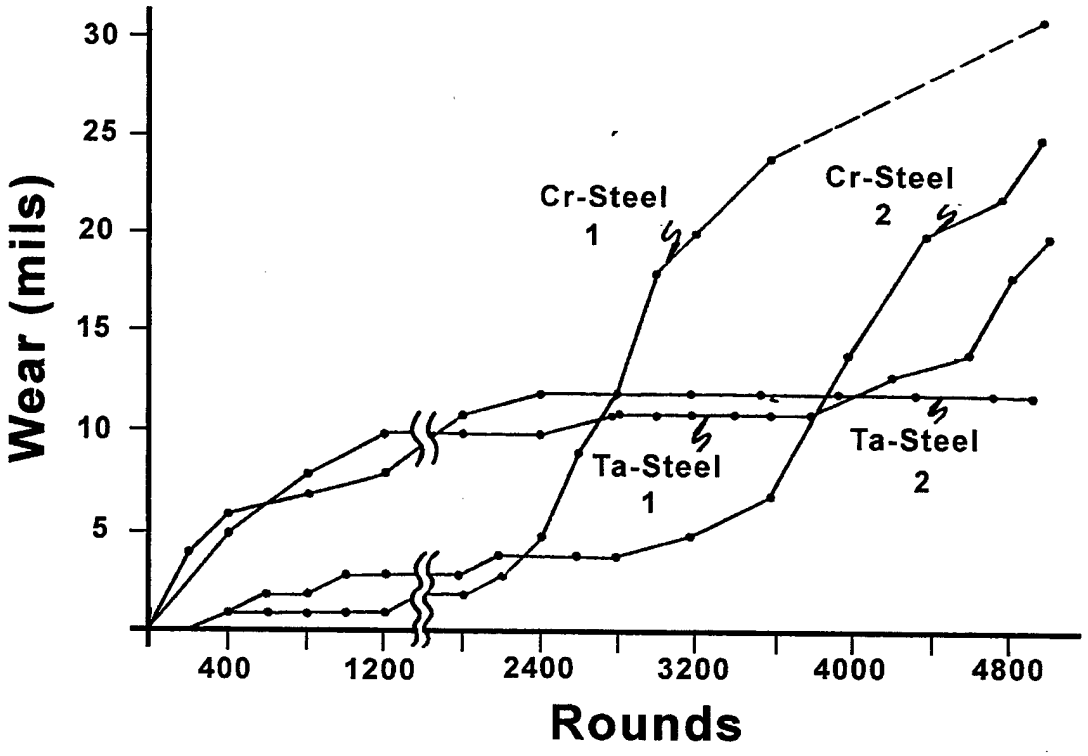

Figure 1. Wear versus rounds in typical electrochemical-deposited tantalum and chromium liners from molten salt.

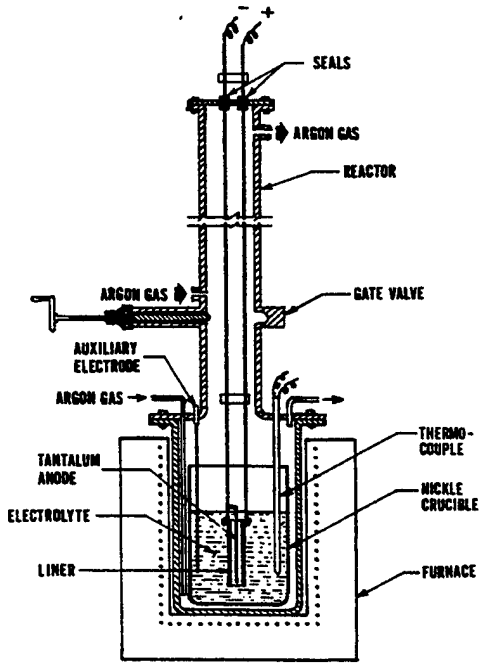

Figure 2a. Electrolyte cell used for molten salt deposition of tantalum-coated steel liners.

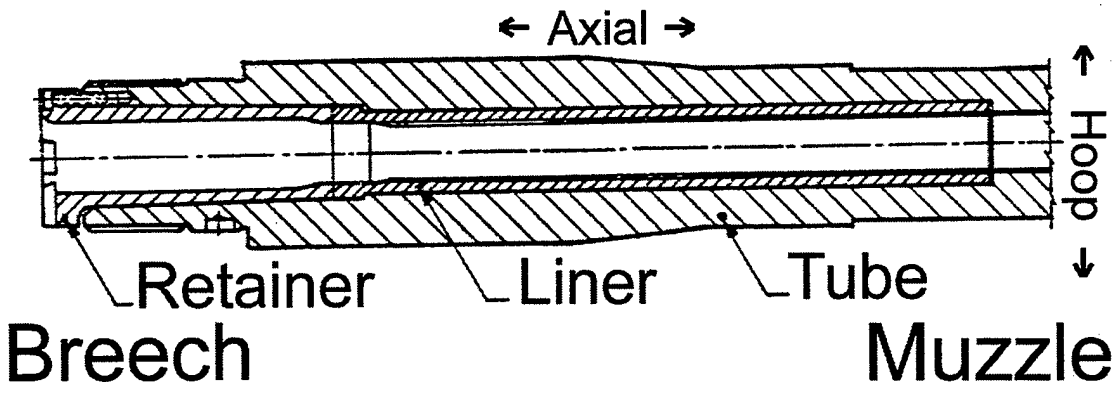

Figure 2b. Liner surface geometry showing breech and muzzle end and axial versus hoop directions.

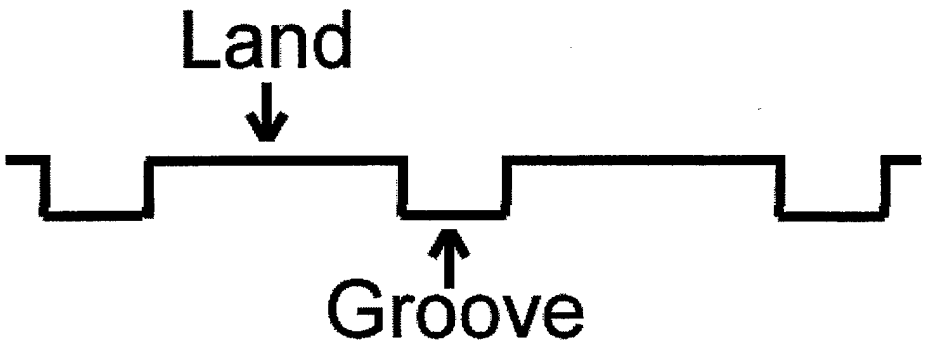

Figure 2c. Schematic of rifling showing the distinction between land and groove.

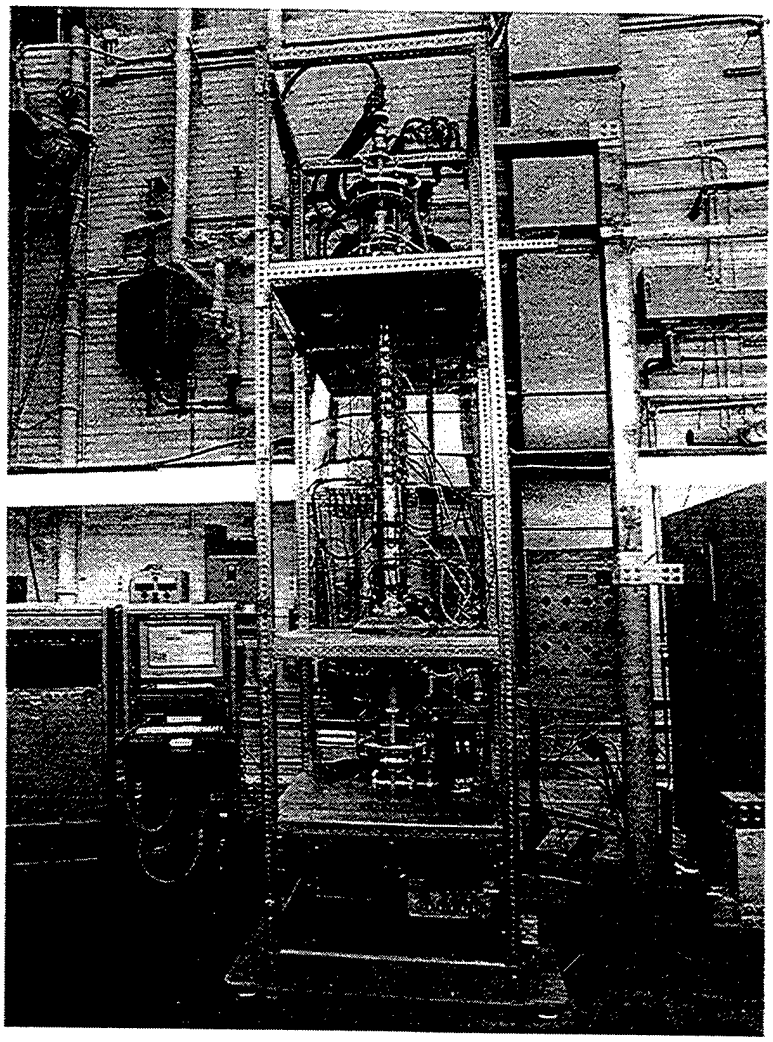

Figure 2d. Schematic of cylindrical magnetron sputtering system for coating interior surfaces of steel cylinders.

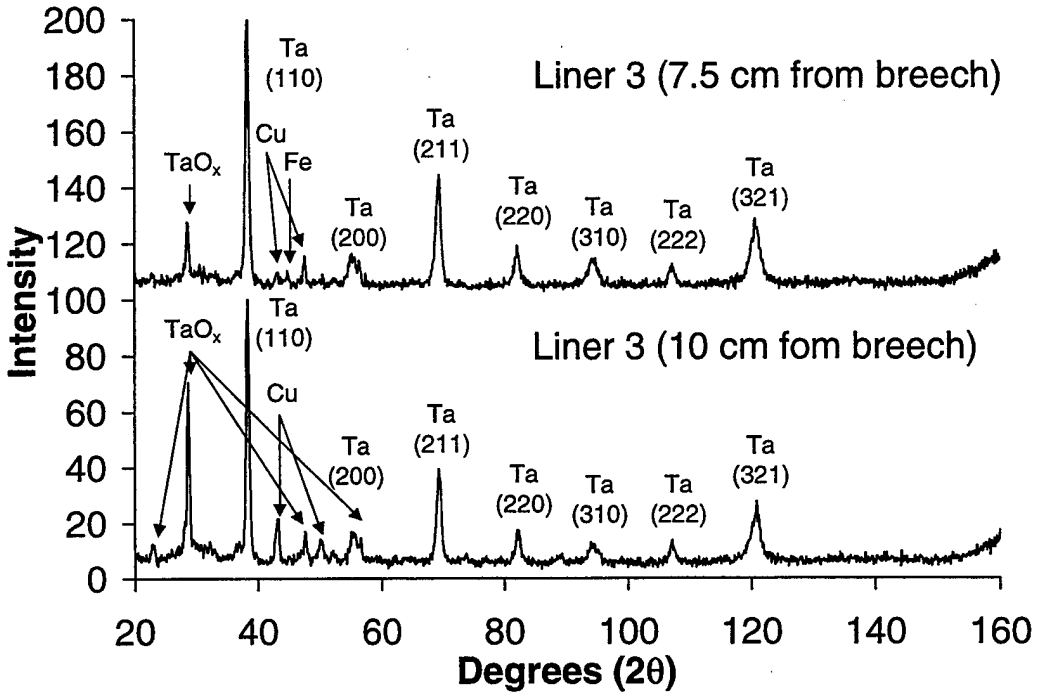

Figure 3a. X-ray diffraction patterns of two specimens cut 7.5-cm and 10-cm from the breech end of Liner 3.

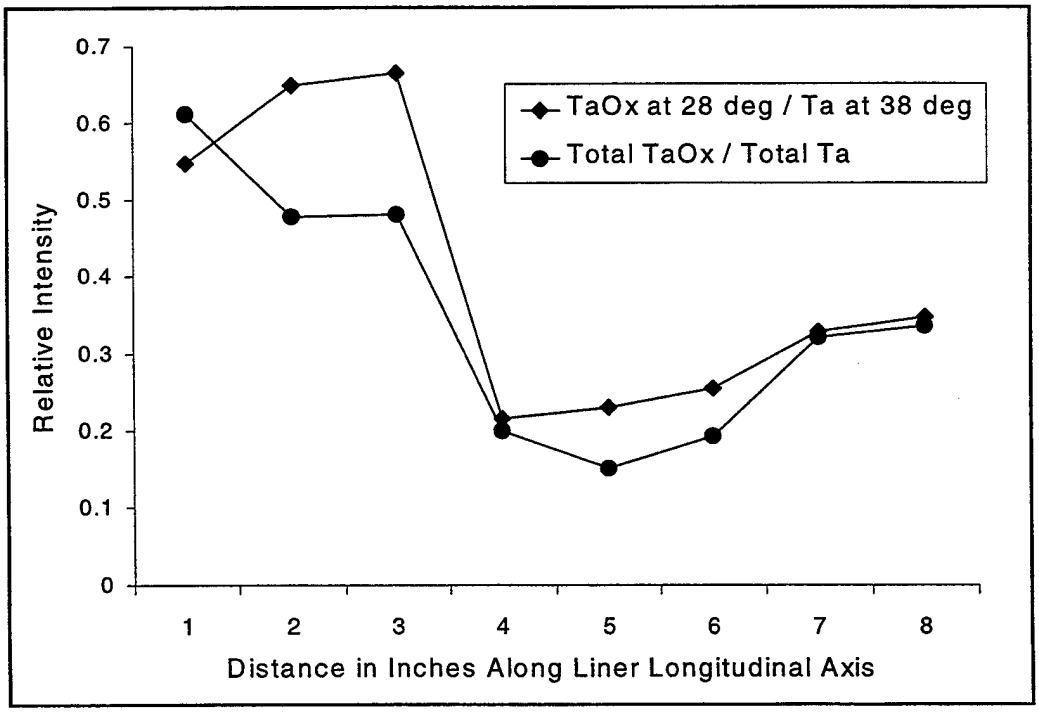

Figure 3b. Ratio of tantalum oxide versus tantalum x-ray intensities as a function of axial distance for Liner 3.

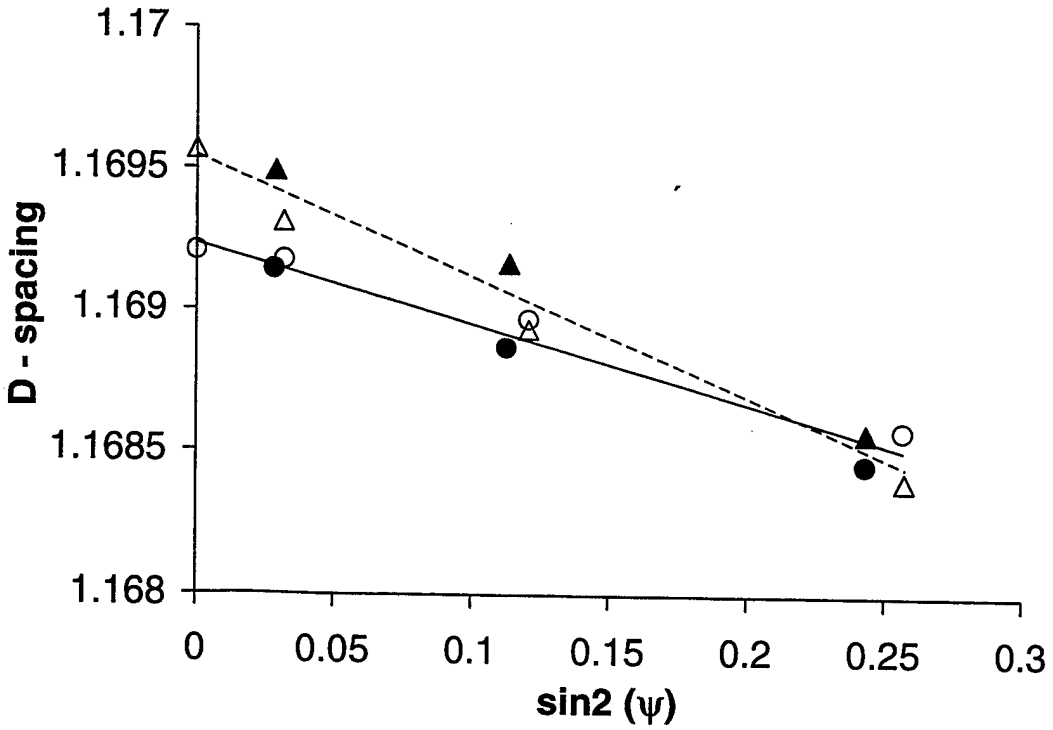

Figure 3c. Residual stress at the breech end and muzzle end of Liner 3. (Triangles represent data at the breech end and dots represent data at the muzzle end.)

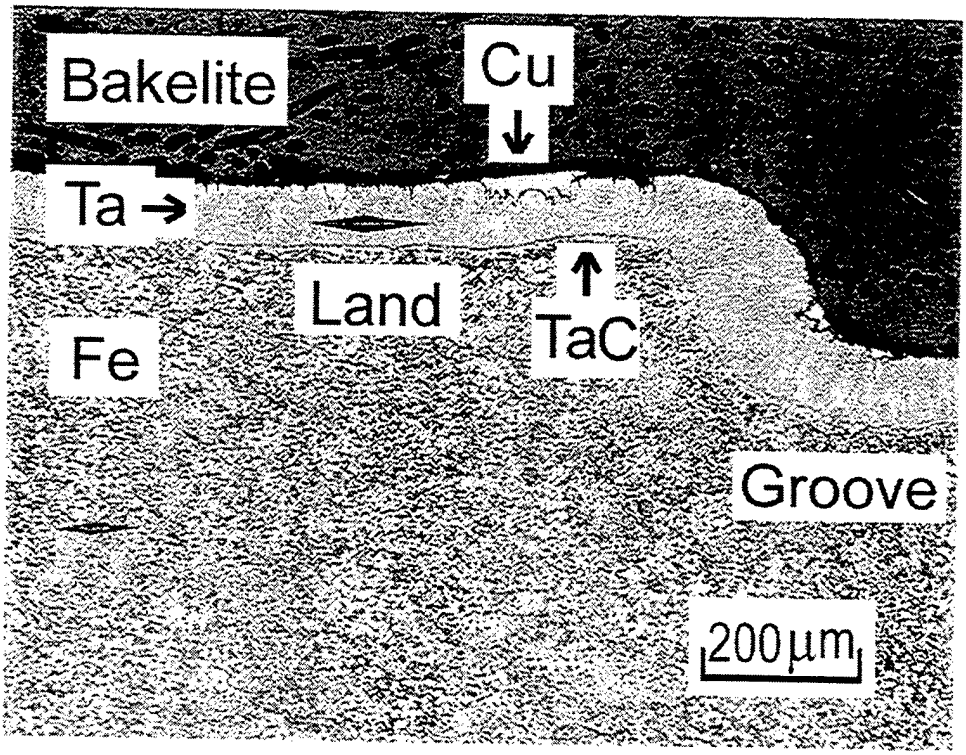

Figure 4a. Photomicrograph of tantalum Liner 1 showing swaging effect of the coatings and surface copper debris.

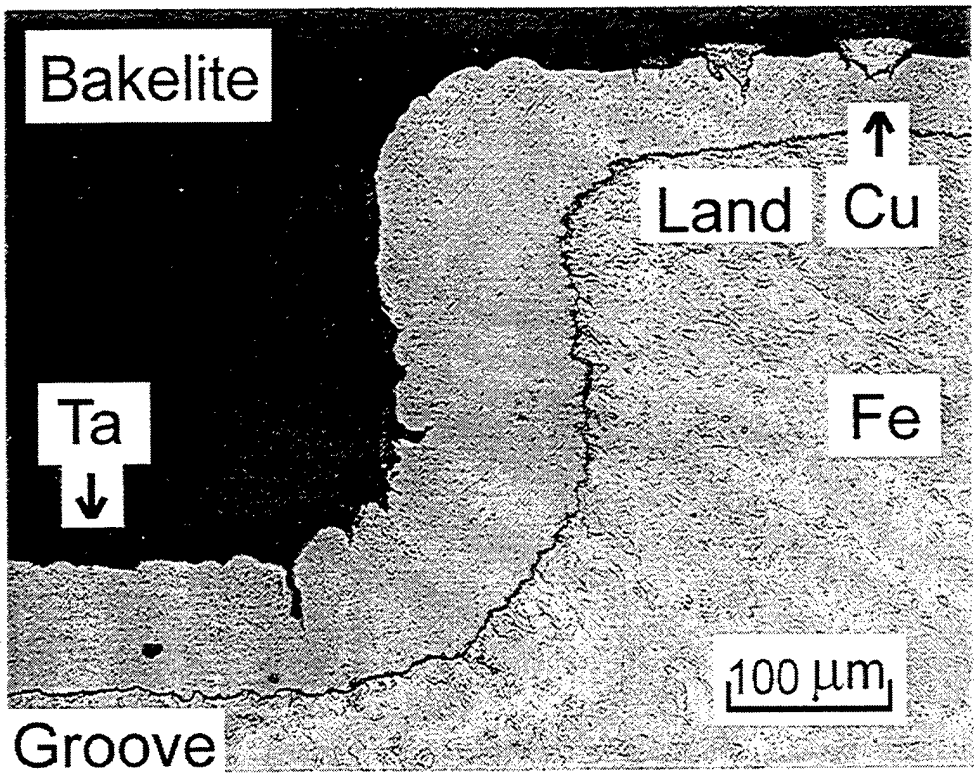

Figure 4b. Photomicrograph of Liner 1 showing crack pattern in tantalum.

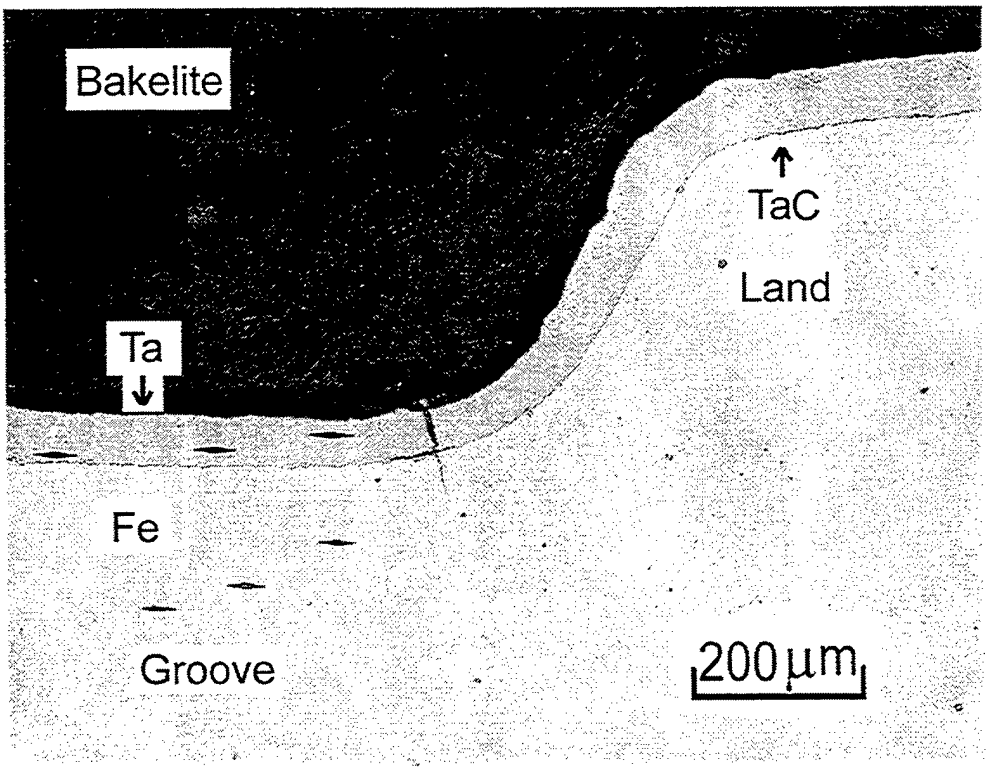

Figure 4c. Photomicrograph of Liner 3.

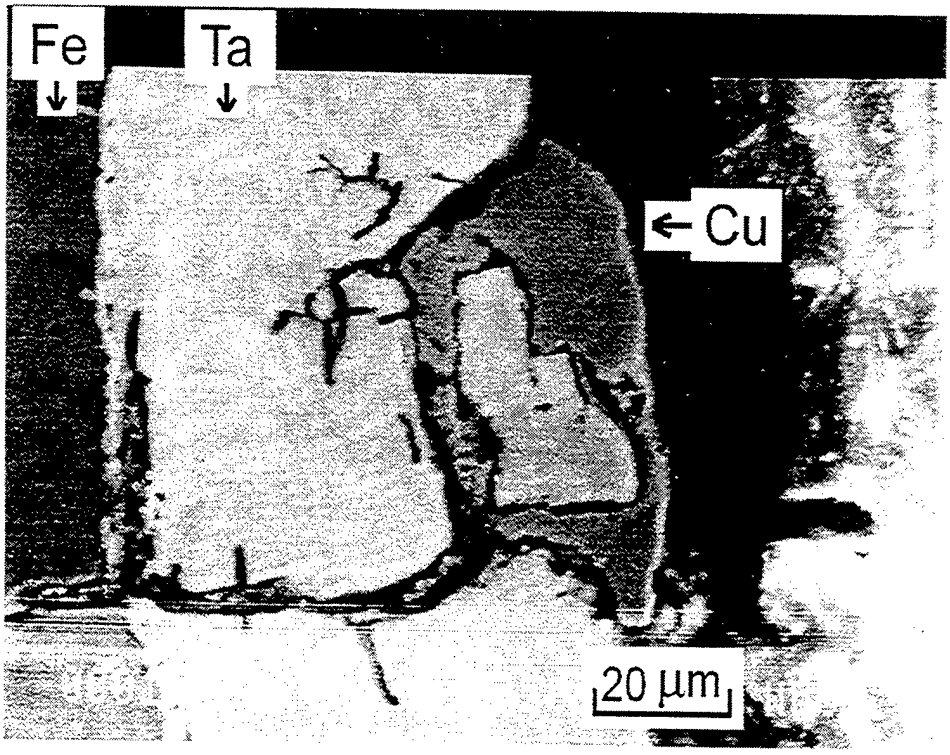

Figure 4d. Scanning electron micrograph depicting a piece of tantalum encased in melted copper.

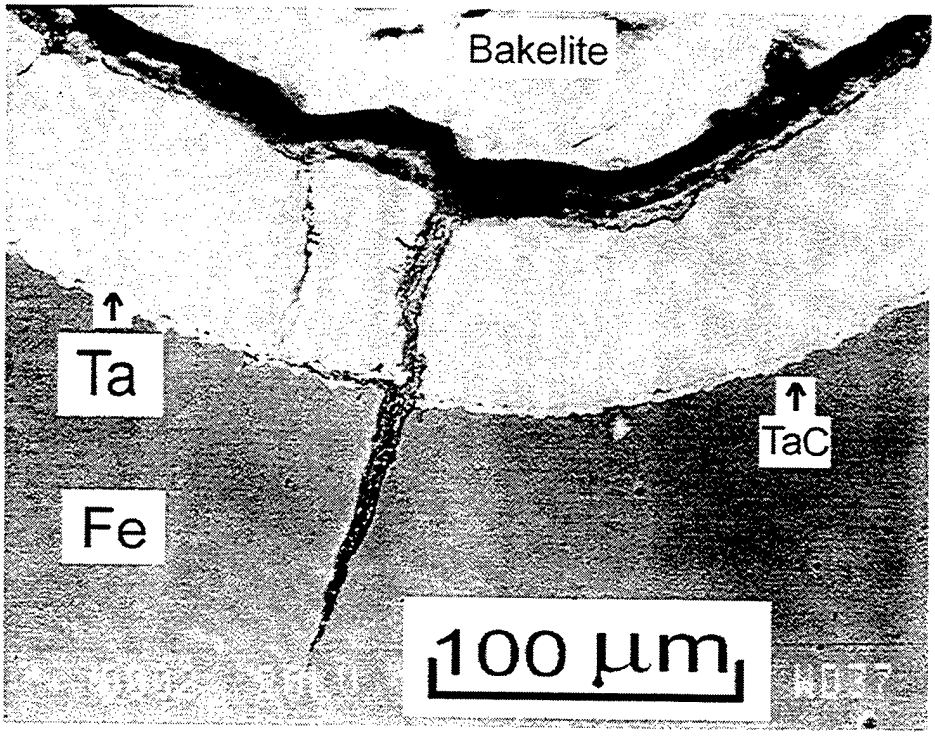

Figure 4e. Scanning electron micrograph depicting crack growth in steel and along the tantalum/steel interface.

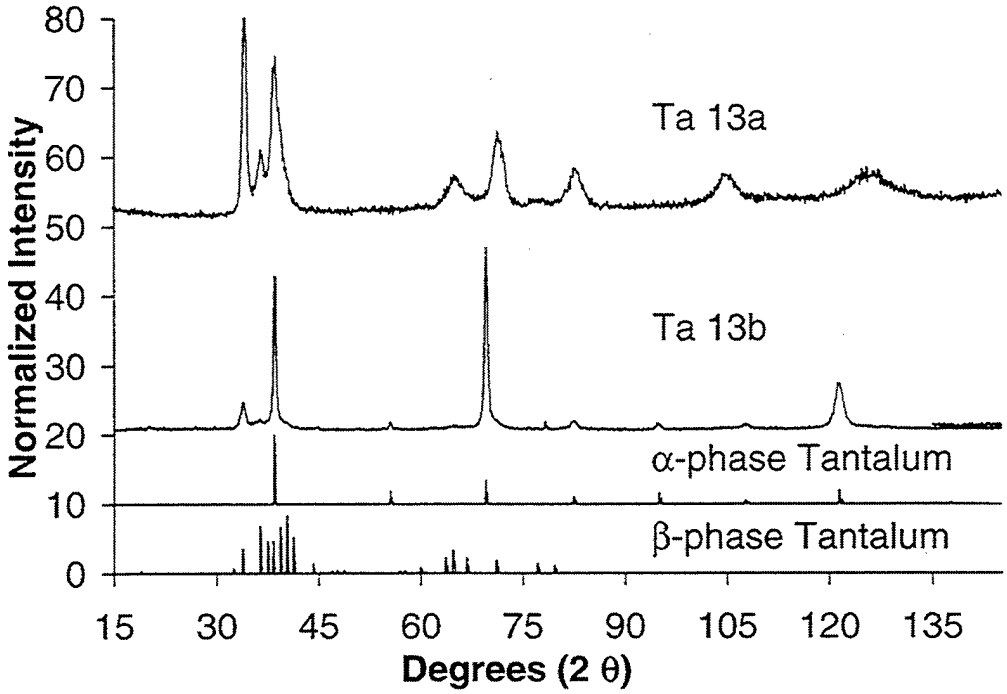

Figure 5a. X-ray diffraction of cylindrical magnetron sputtered Ta13a showing predominant β-phase tantalum with traces of α-phase tantalum, and Ta13b showing α-phase tantalum.

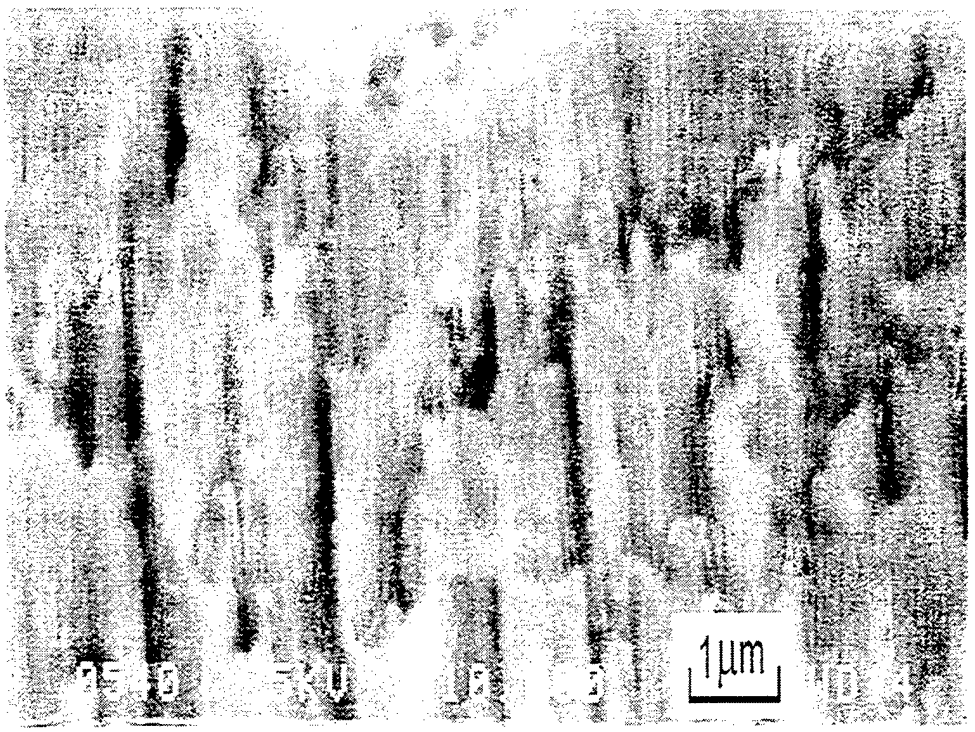

Figure 5b. Scanning electron micrograph of microstructure for Ta13a.

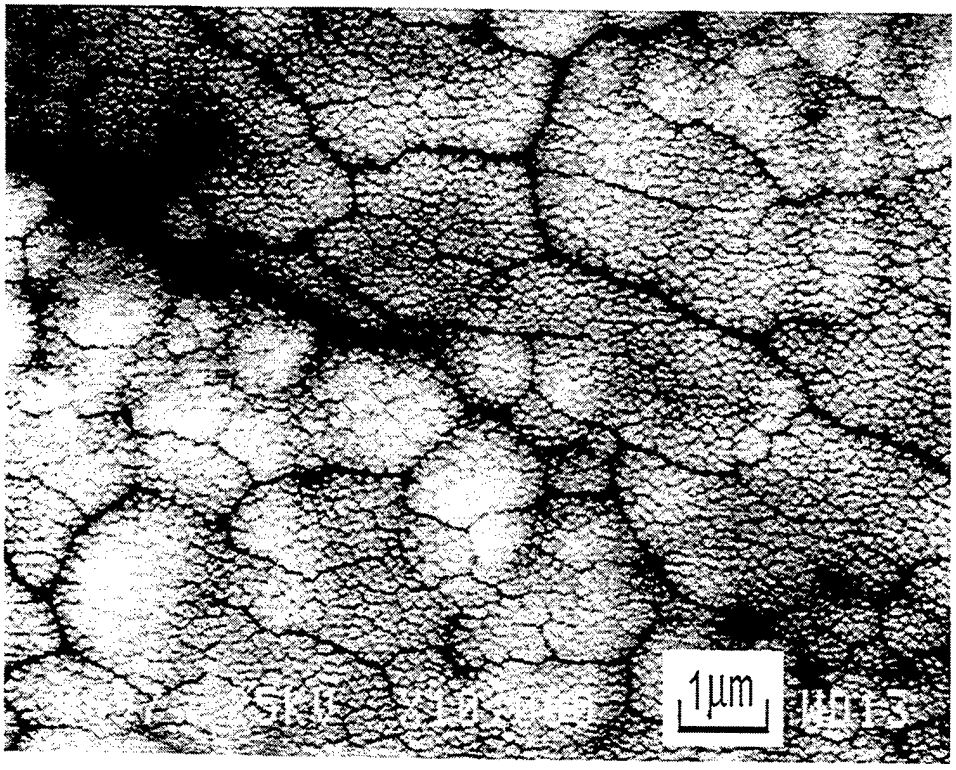

Figure 5c. Topography of Ta13a, including domed tops with large voids.

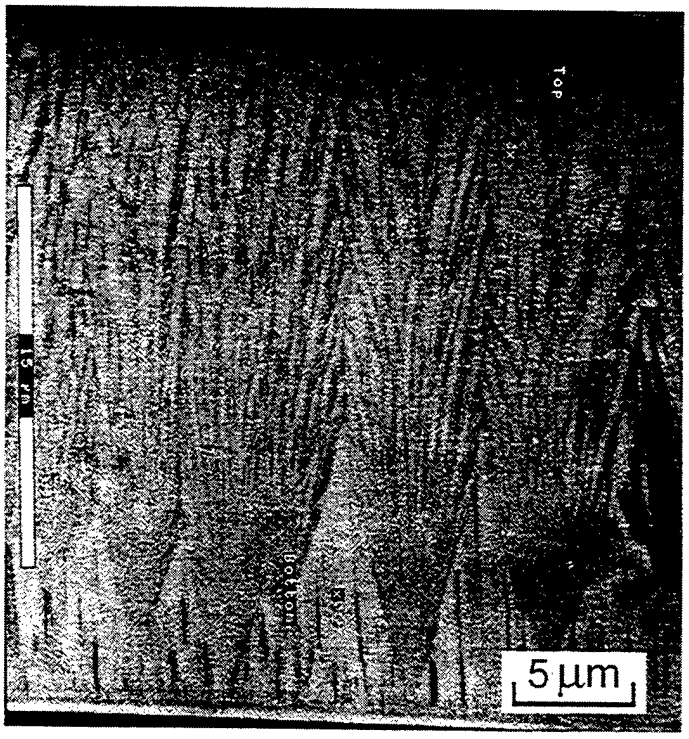

Figure 5d. Cylindrical magnetron sputtered Ta13b microstructure revealing β-phase nucleation at the interface, and growth of α-phase tantalum.

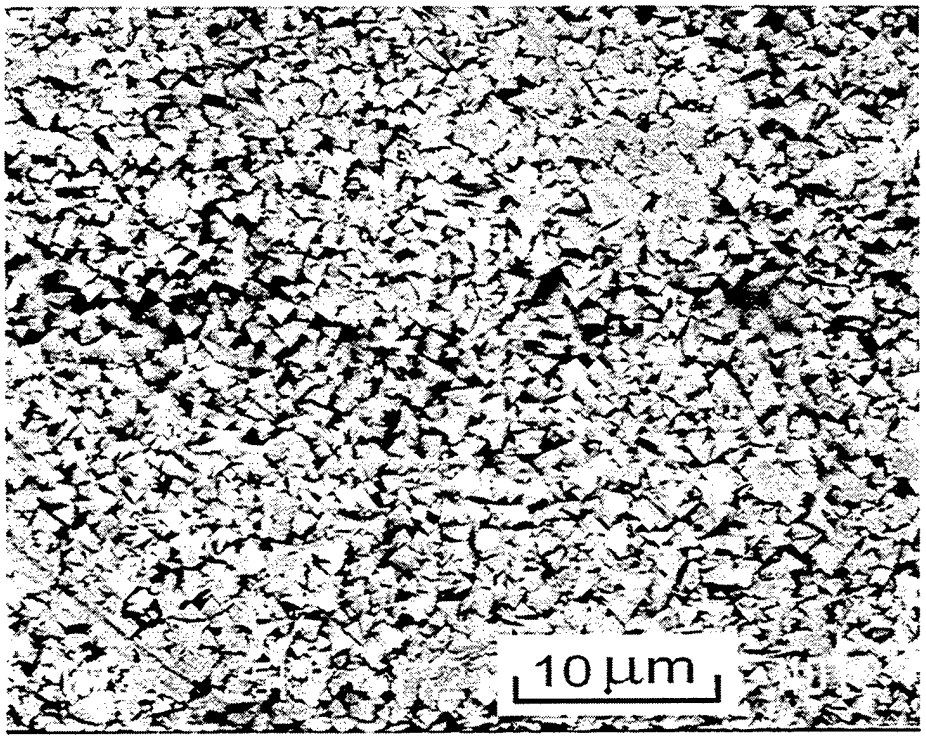

Figure 5e. Topography of Ta13b, including faceted surface.

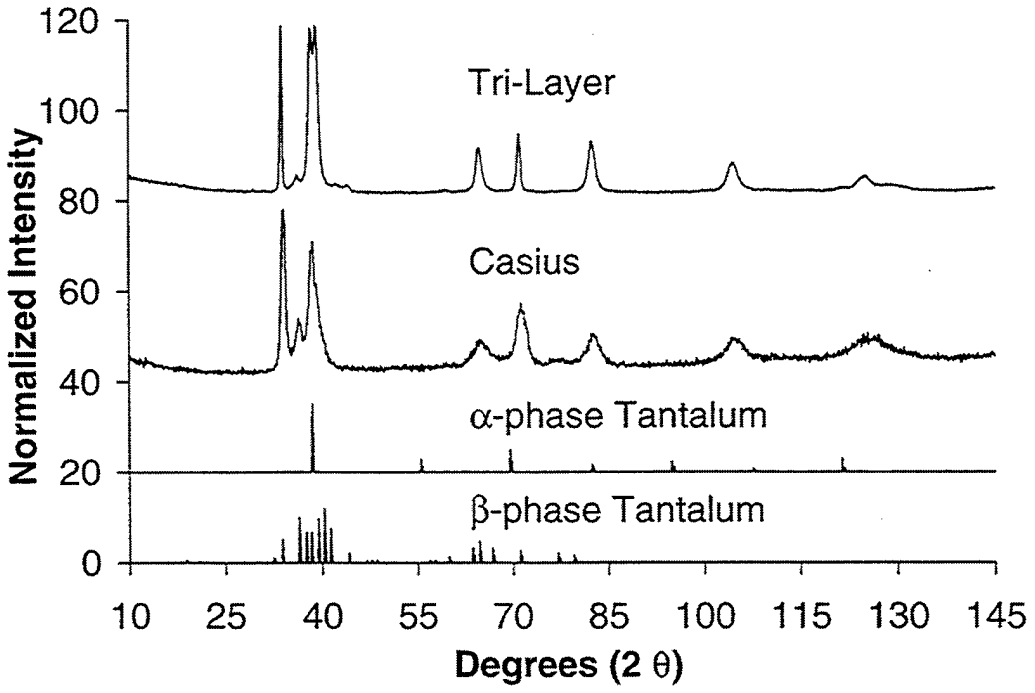

Figure 6a. X-ray diffraction of two cylindrical magnetron sputtered specimens, from a tri-layer coating and a Casius coating.

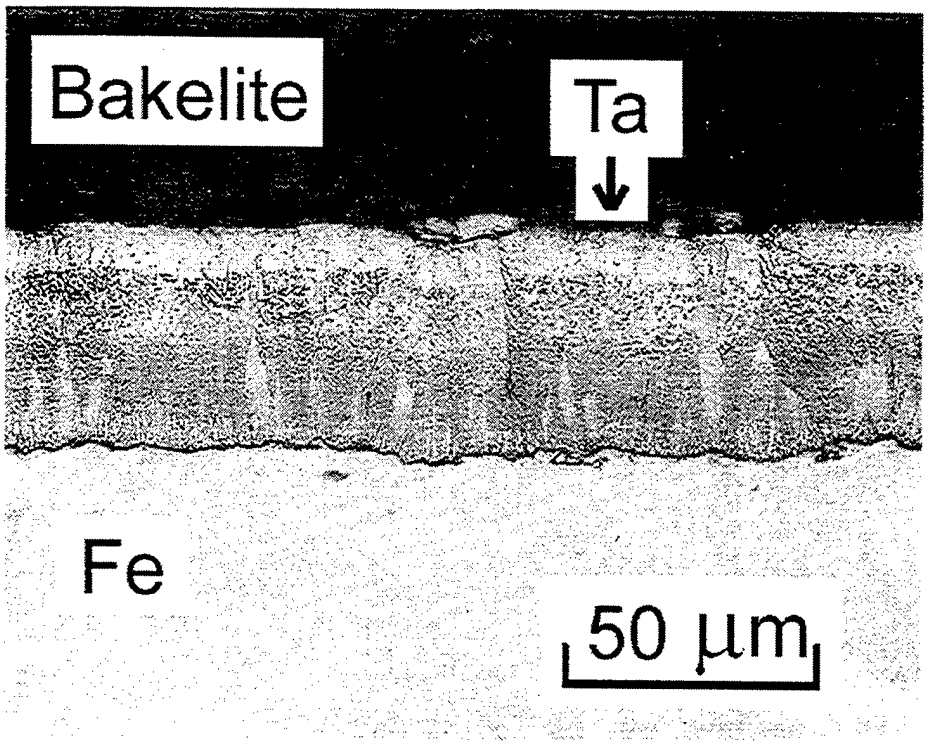

Figure 6b. Photomicrograph demonstrating coating morphology changes with changing argon pressure in the tri-layer coating.

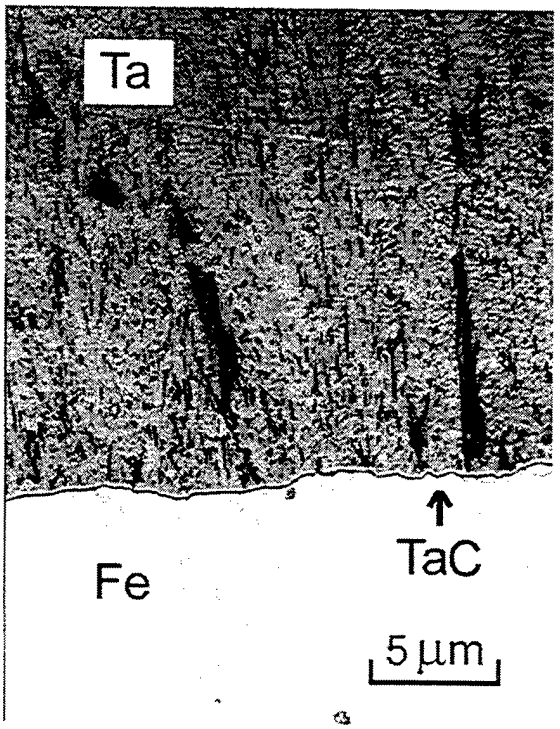

Figure 6c. Laser photomicrograph of specimen taken at 33 Pa (250 mTorr) argon pressure showing coating porosity (1200×).

TECHNICAL REPORT INTERNAL DISTRIBUTION LIST

	NO. OF COPIES
TECHNICAL LIBRARY ATTN: AMSTA-AR-CCB-O	5
TECHNICAL PUBLICATIONS & EDITING SECTION ATTN: AMSTA-AR-CCB-O	3
OPERATIONS DIRECTORATE ATTN: SIOWV-ODP-P	1
DIRECTOR, PROCUREMENT & CONTRACTING DIRECTORATE ATTN: SIOWV-PP	1
DIRECTOR, PRODUCT ASSURANCE & TEST DIRECTORATE ATTN: SIOWV-QA	1

NOTE: PLEASE NOTIFY DIRECTOR, BENÉT LABORATORIES, ATTN: AMSTA-AR-CCB-O OF ADDRESS CHANGES.

TECHNICAL REPORT EXTERNAL DISTRIBUTION LIST

	NO. OF COPIES
DEFENSE TECHNICAL INFO CENTER ATTN: DTIC-OCA (ACQUISITIONS) 8725 JOHN J. KINGMAN ROAD STE 0944 FT. BELVOIR, VA 22060-6218	2
COMMANDER U.S. ARMY ARDEC ATTN: AMSTA-AR-WEE, BLDG. 3022 AMSTA-AR-AET-O, BLDG. 183 AMSTA-AR-FSA, BLDG. 61 AMSTA-AR-FSX AMSTA-AR-FSA-M, BLDG. 61 SO AMSTA-AR-WEL-TL, BLDG. 59 PICATINNY ARSENAL, NJ 07806-5000	 1 1 1 1 1 2
DIRECTOR U.S. ARMY RESEARCH LABORATORY ATTN: AMSRL-DD-T, BLDG. 305 ABERDEEN PROVING GROUND, MD 21005-5066	 1
DIRECTOR U.S. ARMY RESEARCH LABORATORY ATTN: AMSRL-WM-MB (DR. B. BURNS) ABERDEEN PROVING GROUND, MD 21005-5066	 1
COMMANDER U.S. ARMY RESEARCH OFFICE ATTN: TECHNICAL LIBRARIAN P.O. BOX 12211 4300 S. MIAMI BOULEVARD RESEARCH TRIANGLE PARK, NC 27709-2211	 1

	NO. OF COPIES
COMMANDER ROCK ISLAND ARSENAL ATTN: SIORI-SEM-L ROCK ISLAND, IL 61299-5001	 1
COMMANDER U.S. ARMY TANK-AUTMV R&D COMMAND ATTN: AMSTA-DDL (TECH LIBRARY) WARREN, MI 48397-5000	 1
COMMANDER U.S. MILITARY ACADEMY ATTN: DEPT OF CIVIL & MECH ENGR WEST POINT, NY 10966-1792	 1
U.S. ARMY AVIATION AND MISSILE COM REDSTONE SCIENTIFIC INFO CENTER ATTN: AMSAM-RD-OB-R (DOCUMENTS) REDSTONE ARSENAL, AL 35898-5000	 2
COMMANDER U.S. ARMY FOREIGN SCI & TECH CENTER ATTN: DRXST-SD 220 7TH STREET, N.E. CHARLOTTESVILLE, VA 22901	 1

NOTE: PLEASE NOTIFY COMMANDER, ARMAMENT RESEARCH, DEVELOPMENT, AND ENGINEERING CENTER, BENÉT LABORATORIES, CCAC, U.S. ARMY TANK-AUTOMOTIVE AND ARMAMENTS COMMAND, AMSTA-AR-CCB-O, WATERVLIET, NY 12189-4050 OF ADDRESS CHANGES.